

ARTICLE OPEN



Preventing light-induced toxicity in a new mouse model of sector retinitis pigmentosa caused by Rhodopsin M39R variant

Rosellina Guarascio (1) ^{1 ≤ 1}, Kalliopi Ziaka (1) ¹, Kwan-Leong Hau¹, Davide Piccolo¹, Sara Eliza Nieuwenhuis¹, Adriana Bakoulina¹, Rowan Asfahani¹, Monica Aguilà¹, Dimitra Athanasiou¹, Diana Sefic Svara¹, Yumei Li², Rui Chen² and Michael E. Cheetham (1)

© The Author(s) 2025

Retinitis Pigmentosa (RP) is an inherited retinal dystrophy characterised by the progressive loss of rod photoreceptors. Sector RP is a form of RP where degeneration originates in the inferior retina, mainly influenced by light exposure. Over 200 *RHO* variants are pathogenic and associated with autosomal dominant RP. *RHO*^{M39R} is one of the most common *RHO* variants linked to sector RP in the UK. A knock-in (KI) mouse model expressing *Rho*^{M39R} was generated and characterised to investigate the mechanisms of degeneration associated with this variant and explore novel therapeutic strategies for rhodopsin sector RP. Under cyclic ambient light, *Rho*^{M39R/+} KI mice exhibited impaired retinal function by ERG, with some defects in OS ultrastructure, but retained normal outer nuclear layer (ONL) thickness. Repeated exposure to bright light led to photoreceptor loss. In contrast, *Rho*^{M39R/M39R} KI mice in cyclic ambient light displayed severe retinal dysfunction, ONL thinning, and grossly abnormal OS ultrastructure. In homozygous mice, a single bright light exposure significantly reduced ONL thickness within 48 h. The rescue of these models was achieved through reduced light exposure and pharmacological intervention. Rearing in dim red light (red cage condition) restored ERG responses in *Rho*^{M39R/+} KI mice and improved ONL thickness in *Rho*^{M39R/M39R} KI mice. Transcriptomic analysis in *Rho*^{M39R/M39R} KI mice revealed upregulation of Sphingosine 1-P Receptor (*S1pr*) transcripts. Treatment with the S1PR agonist Fingolimod (FTY720) before bright light exposure significantly reduced degeneration, demonstrating a protective effect in both heterozygous and homozygous models and suggesting potential as a therapeutic approach for sector RP patients.

Cell Death Discovery (2025)11:477; https://doi.org/10.1038/s41420-025-02769-2

INTRODUCTION

Retinitis Pigmentosa (RP) is an inherited retinal dystrophy (IRD) that affects 1 in 4000 people globally. RP leads to the dysfunction and loss of rod photoreceptors, followed by the dysfunction and loss of cone photoreceptors [1]. In RP, pigment deposits accumulate initially in the peripheral area, while patients experience night blindness and tunnel vision. In later stages of the disease, the degeneration gradually spreads towards the centre of the retina, leading to a progressive loss of vision and to legal blindness [1, 2]. The progression of the disease can be affected by both genetic and environmental factors, including the exposure of the retina to bright sources of light [3].

RHO was the first gene to be associated with RP [4]. RHO-associated pathology is generally inherited as an autosomal dominant trait [5]. RHO encodes for rhodopsin, the light-sensitive receptor protein of rod photoreceptor cells that plays a crucial role in the visual cycle and in phototransduction. Structurally, rhodopsin is a G-protein-coupled receptor (GPCR), consisting of an opsin protein bound to 11-cis-retinal, a derivative of vitamin A. When light is absorbed, 11-cis-retinal isomerizes to all-trans-retinal, and rhodopsin undergoes a conformational change that triggers the initiation of the phototransduction pathway essential for vision in scotopic (low-light) conditions [6, 7].

Over 200 RHO variants are associated with autosomal dominant forms of RP (adRP). RHO variants can be classified according to

their biochemical and cellular consequences [5]. The best characterised is RHO^{P23H} , a class 2 mutation that causes misfolding and endoplasmic reticulum (ER) retention of the rhodopsin protein [5, 8, 9]. RHO^{P23H} is also the most frequent RHO variant in the US population, with a prevalence of 10-12% among all the adRP cases in the USA [10]. A range of transgenic and knock-in (KI) models have been generated to investigate in vivo the role of Rho^{P23H} in the onset and progression of adRP [11–13].

In the UK population, however, RHO^{P23H} is much less frequently observed, while other less well-studied RHO variants account for most rhodopsin adRP. One of the most common RHO variants in the UK population is RHO^{M39R}. RHO^{M39R} is clinically associated with sector RP, a form of RP where light plays a key role. In sector RP, retinal degeneration initiates in the inferior retina, which is more exposed to bright light from above [14]. The biochemical and cellular effect of M39R on rhodopsin function was studied using heterologous expression, which showed that rhodopsin was not retained in the ER and correctly trafficked to the plasma membrane [15]. However, rhodopsin M39R was expressed at lower levels, and it showed a higher degree of chemical and thermal instability than WT rhodopsin. Interestingly, rhodopsin M39R caused a faster decay of meta-rhodopsin II and a faster rate of activation of transducin [15]. Given these data, RHO^{M39R} was classified as a class 4 rhodopsin variant, with reduced stability of

¹UCL, Institute of Ophthalmology, London, UK. ²UCl, School of Medicine, Irvine, CA, USA. [©]email: rosellina.guarascio.13@ucl.ac.uk

Received: 12 May 2025 Revised: 21 August 2025 Accepted: 8 September 2025

Published online: 21 October 2025

the rhodopsin protein, but the consequences in vivo have not been studied [5].

To investigate the pathogenesis of rhodopsin M39R mediated sector RP, we generated and characterised a *Rho*^{M39R} KI mouse model as a murine model for sector RP. Here, we investigated the impact of manipulating light exposure on photoreceptor ultrastructure and survival in *Rho*^{M39R} KI mice. Transcriptomic analyses highlighted altered pathways for pharmacological targeting to reveal how molecular interventions can influence the progression of rhodopsin M39R-induced pathology and identify new potential therapeutic approaches.

RESULTS

Generation of Rho^{M39R} mice

The *Rho*^{M39R} KI mouse model was generated using homologous-directed repair (HDR) CRISPR/Cas9 technology by electroporating C57BL/6J mouse embryos with a guide RNA (gRNA) and a donor sequence containing nucleotide substitutions for the *Rho* gene [16]. A substitution of thymine to guanine at coding position 116 results into an amino acid change from methionine to arginine in position 39, located in the first transmembrane helix (TM) of rhodopsin (Supplementary Tables 1 and 2). A second substitution was introduced to modify the protospacer adjacent motif (PAM) site and consequently to inhibit repeated Cas9 DNA cleavage (Supplementary Tables 1 and 2). Embryos were then reintroduced into a pseudo pregnant mother to generate edited mice. The founder *Rho*^{M39R/+} KI mouse was identified by Sanger sequencing. *Rho*^{M39R/+} mice were backcrossed with C57BL/6J mice for at least 6 generations to reduce the risk of off-targets effects before performing further experiments (Supplementary Table 3).

The effect of Rho^{M39R} expression on photoreceptor survival and function

To investigate the role of rhodopsin M39R on photoreceptor survival and retina activity, Rho^{M39R} KI mice reared in ambient cyclic light were characterised by optical coherence tomography (OCT), electroretinogram (ERG) (Supplementary Fig. 1) and immunohistochemistry (IHC) (Fig. 1 and Supplementary Fig. 2). Live images of the central retina were acquired by OCT to measure the outer nuclear layer (ONL) thickness (Fig. 1A and Supplementary Fig. 2A). Heterozygous $Rho^{M39R/+}$ mice had a slightly thinner ONL in the inferior retina at 5 months compared to $Rho^{+/+}$ mice (Supplementary Fig. 2A), but no difference was detected at 3 weeks (Fig. 1A and Supplementary Fig. 1). In contrast, homozygous $Rho^{M39R/M39R}$ mice showed a significant reduction of the ONL thickness already by 3 weeks of age (Fig. 1A and Supplementary Fig. 1).

Although $Rho^{M39R/+}$ mice had no change in photoreceptor survival at 3 weeks, a significant reduction in their light response was detected. Scotopic A and B waves were reduced in $Rho^{M39R/+}$ compared to $Rho^{+/+}$ mice retinae (Fig. 1B and Supplementary Fig. 1B). Furthermore, $Rho^{M39R/M39R}$ KI mice exhibited a greater deficit in the light response, with scotopic A and B waves values significantly lower than both $Rho^{M39R/+}$ and $Rho^{+/+}$ mouse retina (Fig. 1B and Supplementary Fig. 1B).

The effect of $\mathit{Rho}^{\mathit{M39R}}$ on rhodopsin expression and photoreceptor structure

Rhodopsin localised in the outer segment (OS) in both $Rho^{M39R/+}$, at 3 weeks and 5 months, and $Rho^{M39R/M39R}$ models, similar to control retina (Fig. 1C and Supplementary Fig. 2). By contrast, rhodopsin staining in homozygous mice was also detectable in the rod photoreceptor cell bodies (Fig. 1C).

Rho^{P23H} mice have altered OS discs formation and orientation associated with an impaired ERG [13, 17]. Therefore, we investigated the ultrastructure of rod photoreceptor OS in Rho^{M39R}

models by Transmission Electron Microscopy (TEM) at 3 weeks of age (Fig. 1D). $Rho^{M39R/+}$ rod OS were generally comprised of tightly packed discs, similar to $Rho^{+/+}$ OS. Nevertheless, disorganised areas characterised by transversally oriented discs intercalated with vesicular structures were also observed frequently in the $Rho^{M39R/+}$ rod OS (Fig. 1D). Control wild-type rod OS occasionally had transversally oriented discs, as already described [13, 17]; however, the percentage of rod OS with disorganised areas was significantly increased in $Rho^{M39R/+}$ retinae (Supplementary Fig. 3A, B), and OS vesicular structures were only observed in $Rho^{M39R/+}$ mice (Fig. 1D). Furthermore, the OS diameter was significantly smaller by approximately 20% in $Rho^{M39R/+}$ compared to control mice. The average diameter was $1.38 \pm 0.10 \, \mu m$ in $Rho^{+/+}$ OS, while only $1.13 \pm 0.15 \, \mu m$ in $Rho^{M39R/+}$ OS (Supplementary Fig. 3C).

Several studies have shown that a difference in OS diameter can be associated with by reduced levels of rhodopsin expression [18, 19]. The protein level of rhodopsin in $Rho^{M39R/+}$ mice was measured by western blot; however, no difference in rhodopsin levels was observed in $Rho^{M39R/+}$ mice compared to $Rho^{+/+}$ mouse retinal lysates (Supplementary Fig. 4A, B).

In contrast, $Rho^{M39R/M39R}$ OS were very disrupted with an

In contrast, *Rho*^{M39R/M39R} OS were very disrupted with an abnormal orientation and compactness of the discs (Fig. 1D). Vesicular structures were also observed. Immunoblot analysis showed that the level of rhodopsin was around 70% lower than in *Rho*^{+/+} animals (Supplementary Figs. 4A, B and 14).

These data show that despite rhodopsin M39R traffic to the OS in *Rho*^{M39R} models, photoreceptor function is impaired compared to controls, and there is a defect in OS disc organization that is more severe in homozygous mice. In addition, *Rho*^{M39R/M39R} had retinal degeneration by 3 weeks of age.

The role of bright light in Rho^{M39R} mediated degeneration

RHO^{M39R} variant is association with sector RP, a form of RP where light is thought to play a critical role [14]. Therefore, we hypothesised that light could accelerate dysfunction and degeneration in Rho^{M39R} mice. In order to assess Rho^{M39R} photosensitivity, $Rho^{M39R/+}$ mice were exposed to repeated ERG with a last step of light intensity set up to 30 k lux (Fig. 2A). The first ERG was performed on dark-adapted mice at 3 weeks of age, and the ERG was repeated 2 and 4 weeks later on the same mice. The ONL thickness was measured by OCT as a marker of photoreceptor degeneration. Importantly, the photoreceptor layer was significantly thinner after each round of ERG (Fig. 2B). After three ERGs, the ONL thickness of $Rho^{M39R/+}$ mice reached 15–20 µm, equivalent to a few layers of photoreceptors (Fig. 2B, D). The ERG mediated light exposure significantly reduced the ONL thickness of Rho^{M39R/+} mice compared to age-matched Rho^{M39R/+} mice reared in ambient cyclic light only at 7 weeks of age (Fig. 2C, D). Moreover, the repeated light exposure induced a further decline in photoreceptor function in Rho^{M39R/+} mice, as shown by reduced scotopic A wave amplitude compared to mice reared in ambient light (Fig. 2C). There was no change in ONL thickness and photoreceptor activity over 4 weeks in the ambient light only mice. The same paradigm of repeat ERGs on control Rho⁺⁷⁺ mice did not induce degeneration or reduced photoreceptor function (Supplementary Fig. 5A, B).

The same repeat ERG light damage paradigm was also performed on homozygous *Rho*^{M39R/M39R} mice. Initially, the first ERG was performed on mice at 3 weeks of age and repeated after a week. However, a week later, the photoreceptor layer was greatly reduced when imaged by OCT (data not shown). Therefore, a single ERG was performed, and the retinae were collected at 3, 6, and 24 h after the bright light exposure (Fig. 3A). No changes in the ONL thickness were observed by IHC 3 or 6 h after bright light exposure. There was an increase in TUNEL reactivity after 3 and 6 h, but this was not statistically significant (Fig. 3B–D). Whereas ultrastructural investigation by TEM showed that swollen

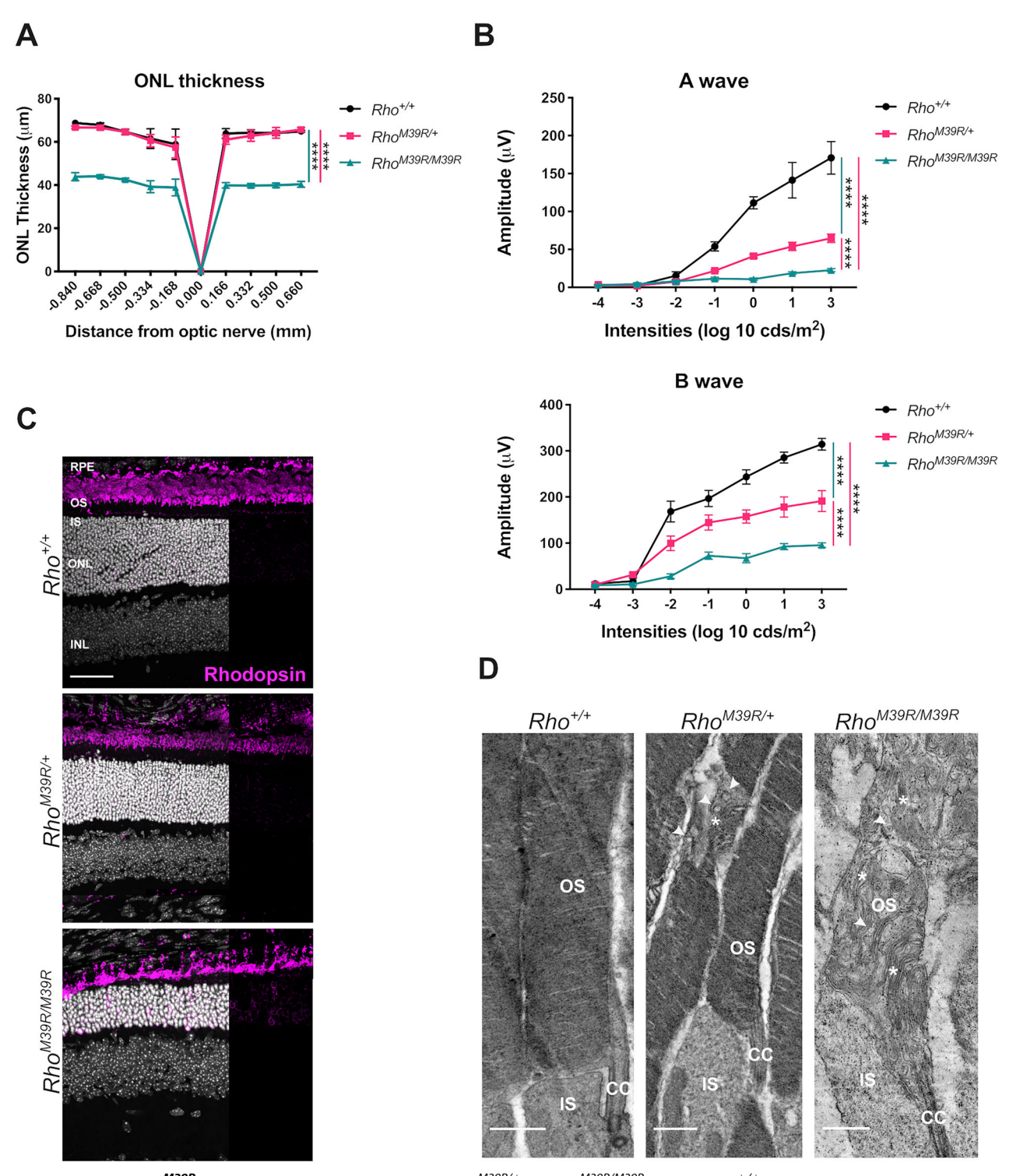


Fig. 1 The effect of Rho^{M39R} expression on photoreceptors. $Rho^{M39R/+}$ KI, $Rho^{M39R/M39R}$ KI, and $Rho^{+/+}$ KI mouse models were analysed by OCT, ERG, IHC, and TEM at 3 weeks of age. **A** The ONL thickness was measured by OCT in the central retina. Mean ± SEM. Two-way ANOVA. Tukey's multiple comparisons test between groups. (****p < 0.0001). N = 4. **B** The activity of the retina was measured by ERG. The A wave reflects the photoreceptors hyperpolarisation in response to different intensities of light and was plotted as positive values. The B wave shows the response of the inner layer of the retina following phototransduction. Mean ± SEM, Two-way ANOVA. Tukey's multiple comparisons test between groups. (****p < 0.0001). N = 4 **C** Mouse retinae were fixed in 4% PFA for 24 h, incubated in 30% sucrose for 1–2 days, embedded in OCT, cryosectioned, and stained with Rhodopsin-4D2 antibody (in magenta). Images were acquired by a Leica Stellaris 8 confocal microscope. Scale bar = 50 μm. **D** The TEM showed the ultrastructure of the OS in the three different models. Stars indicate transversally orientated discs, while arrowheads indicate vesicular structures. Scale bar = 1 μm. OS = Outer Segment, CC = connecting cilium, IS = Inner Segment.

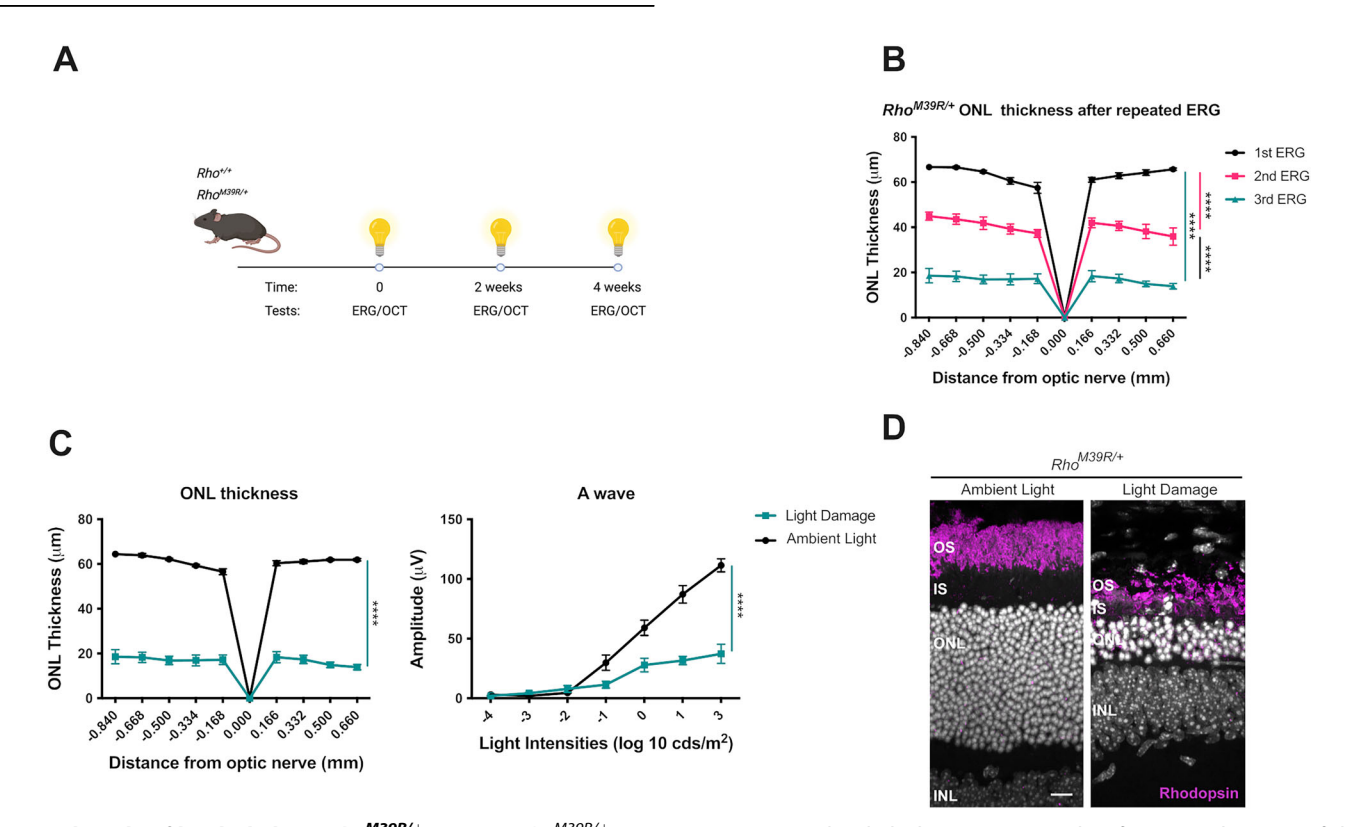


Fig. 2 The role of bright light in $Rho^{M39R/+}$ KI mice. $Rho^{M39R/+}$ KI mice were exposed to light by ERG at 3 weeks of age. A Schematic of the light damage assay in $Rho^{M39R/+}$ KI mice. The animals were dark adapted overnight prior to perform the ERG. The ERG was performed for a total of three times, followed by OCT to image the retina and determine the ONL thickness. **B** The ONL thickness of the $Rho^{M39R/+}$ KI mouse retinae was plotted for each round of ERG. Mean \pm SEM. Mixed-effect ANOVA. Tukey's multiple comparisons test between groups. (***p < 0.001). N = 4 **C** $Rho^{M39R/+}$ KI mice from the light damage assay were compared to animals reared in ambient light to show the difference in ONL thickness and photoreceptors activity (A wave). Mean \pm SEM. Two-way ANOVA (****p < 0.0001). N = 4. **D** IHC of the retina of $Rho^{M39R/+}$ KI mouse after light damage or reared in ambient light. The cryosections were stained with rhodospin-4D2 antibody (in magenta). Scale bar = $10 \mu m$.

mitochondria with disrupted cristae were present in the IS of photoreceptors from 3 h after bright light exposure. The alteration in mitochondrial morphology was exacerbated at 6 h (Supplementary Fig. 6). Shorter OS full of vesicular structures were also observed in *Rho^{M39R/M39R}* mice retina after light exposure (Supplementary Fig. 6). Furthermore, by 24 h after bright light ONL thickness had significantly reduced, together with a significant increase in TUNEL reactivity (Fig. 3B-D). These data confirm that *Rho^{M39R}* mice are sensitive to light to the extent that a short exposure to bright source of light can induce photoreceptor cell death.

Dim red light protection against Rho^{M39R}

In order to test the role of ambient light in photoreceptor dysfunction and degeneration, Rho^{M39R} mice were reared in red cages. Rhodopsin is not activated by red light, and rodents do not express an L cone opsin, therefore, rodents do not show any visual activity under diminished red light, and they can be reared in red cages as if they were living in absence of light [20]. $Rho^{M39R/+}$ mice were reared in dim red light from birth until 3 weeks of age and then characterised. The ONL of $Rho^{M39R/+}$ mice reared in dim red light was significantly thicker than the ONL thickness of $Rho^{M39R/+}$ mice or control mice reared in ambient light (Fig. 4A). In addition, there was a significant improvement of the scotopic A and B wave amplitude in the $Rho^{M39R/+}$ animals reared in dim red light compared to $Rho^{M39R/+}$ mice reared in ambient light. The amplitude of both A and B waves was fully rescued and comparable to the ERG of $Rho^{+/+}$ mice (Fig. 4B). Investigation by TEM revealed that the OS ultrastructure of red cage reared $Rho^{M39R/+}$ mice was improved, with less frequent

breaks observed along the OS compared to animals reared in ambient light (Fig. 4C, D).

Rhodopsin localisation was also investigated in the retina of *Rho*^{M39R/+} mice reared in ambient light and dim red light. The relative fluorescence intensity of rhodopsin staining in the OS was measured in comparison to other compartments (Fig. 4E–G). Interestingly, the rhodopsin OS/IS ratio was significantly higher in the mice reared in dim red light compared to mice reared in ambient light (Fig. 4F). No change in OS length was observed (Fig. 4G). In summary, ambient light can affect rod photoreceptor activity, rhodopsin localisation, and OS structure in *Rho*^{M39R/+} mice.

Rearing in red cages was also tested in *Rho^{M39R/M39R}* mice. Importantly, a significant increase in the ONL thickness was observed in *Rho^{M39R/M39R}* mice reared in red cages compared to ambient light-reared *Rho^{M39R/M39R}* mice (Fig. 5A). Nevertheless, ERG analysis did not show any improved retinal function, even though by TEM, we observed an improvement in the OS ultrastructure. *Rho^{M39R/M39R}* mice reared in dim red light showed short OS composed of tight and evenly arranged discs (Fig. 5C). *Rho^{M39R/M39R}* mice raised in ambient light had some rhodopsin

Rho^{M39R/M39R} mice raised in ambient light had some rhodopsin immunoreactivity in the IS and in the ONL (Fig. 5D). The retention of rhodopsin M39R in the IS was partially rescued in the retina of mice reared in dim red light as shown by a significant improvement in the OS/IS ratio (Fig. 5E). Moreover, Rho^{M39R/M39R} reared in dim red light displayed a longer OS than mice reared in ambient light (Fig. 5F). Therefore, ambient light appears to contribute to photoreceptor degeneration in Rho^{M39R/M39R} mice.

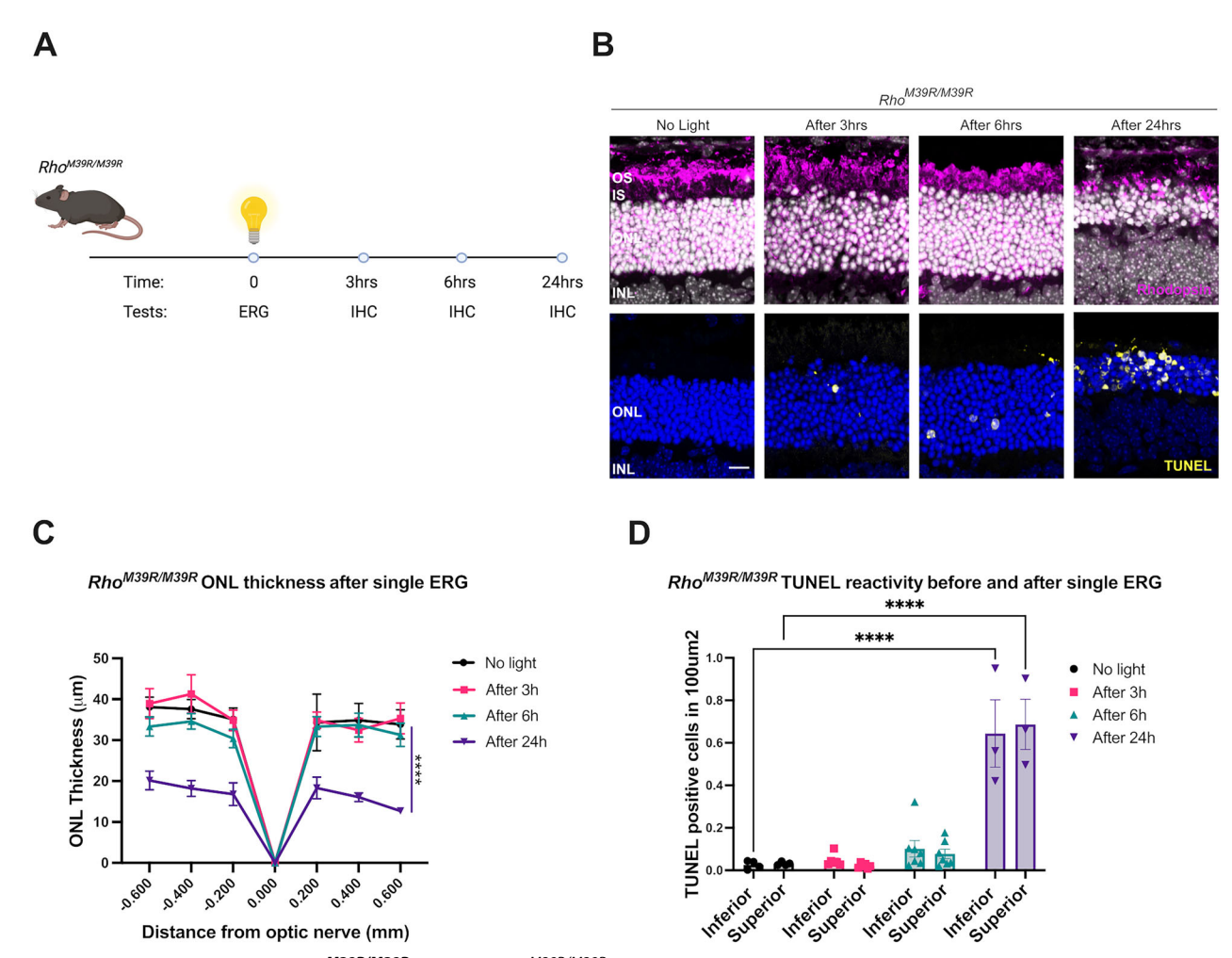


Fig. 3 The role of bright light in $Rho^{M39R/M39R}$ KI mice. $Rho^{M39R/M39R}$ KI mice were exposed to light by ERG at 3 weeks of age. A Schematic of the light damage assay in $Rho^{M39R/M39R}$ KI mice. Mice were dark adapted overnight prior to perform the ERG. The ERG was performed only once. The animals were culled at different time points (3, 6, 24 h after light), and one eye was collected for IHC. **B** Mouse retinae were fixed overnight in 4% PFA, incubated in 30% sucrose for 1–2 days, embedded in OCT (embedding matrix), cryosectioned, and stained with Rhodopsin-1D4 antibody (in magenta) or used for a fluorochrome-based TUNEL assay (in yellow). Images were acquired using a Zeiss LSM700 confocal microscope. Scale bar = 10 μ m **C** Images of the central retina, including the optic nerve, were acquired with an EVOS FL auto 2 microscope and used to measure the ONL thickness at specific distances from the optic nerve comparable to the OCT analysis. Mean \pm SEM. Two-way ANOVA. Tukey's multiple comparisons test between groups. (****p < 0.0001). **D** The number of TUNEL positive cells in the ONL was counted using images of the central retina acquired with an EVOS FL auto 2 microscope. Mean \pm SEM. Two-way ANOVA. Tukey's multiple comparisons test between groups. (****p < 0.0001). No light N = 4, after 3 h N = 6, after 6 h N = 7, after 24 h N = 3.

Altered sphingosine pathway transcripts in *Rho*^{M39R/M39R}

To investigate the transcriptomic changes associated with retinal degeneration driven by Rho^{M39R} , we performed bulk RNA-sequencing (RNA-seq) and compared gene expression of 3-week-old $Rho^{+/+}$ and $Rho^{M39R/M39R}$ mice. The top differentially expressed genes (DEGs) included genes involved in the inflammatory response and complement activation (Fig. 6A). Gene Set Enrichment Analysis (GSEA) using WebGestalt was performed to interpret the upregulated and downregulated DEGs and explore biological processes and pathways involved in retinal degeneration. This confirmed a significant upregulation of inflammatory pathways and a significant downregulation of the phototransduction cascade (Supplementary Fig. 7A, B). Immunohistochemistry showed an infiltration of Iba1 positive cells in the ONL of $Rho^{M39R/M39R}$ mice reared in ambient light compared to both $Rho^{M39R/+}$ and $Rho^{+/+}$ mice (Supplementary Fig. 8A, B), confirming the inflammatory response detected in the transcriptomics.

Interestingly, genes involved in the sphingolipid signalling pathways were also upregulated in the transcriptomic analysis (Fig. 6A and Supplementary Fig. 7C). S1pr3, S1pr2, and Tnfrsf1a were significantly upregulated in Rho^{M39R/M39R} compared to control retinae (Fig. 6A and Supplementary Fig. 7C). Sphingosine-1-phosphate (S1P) is a sphingolipid that act as a lipid mediator and can modulate several cellular processes, including mechanisms of survival and proliferation [21]. High levels of S1P and of S1P receptors (S1pr) have been associated with light damage in other animal models [22-24]. Single cell RNA sequencing (scRNAseq) data previously generated from wild-type mouse retina show that S1pr2 is expressed in Müller cells, astrocytes, and pericytes, whereas the levels of S1pr3 are higher and S1pr3 is mainly expressed in Müller cells and pericytes (Supplementary Fig. 7D) [25]. Reduction of phototransduction protein gene expression could be related to the retinal degeneration occurring in *Rho*^{M39R/M39R} mice; however, upregulation of sphingolipid signalling pathways suggested they could be



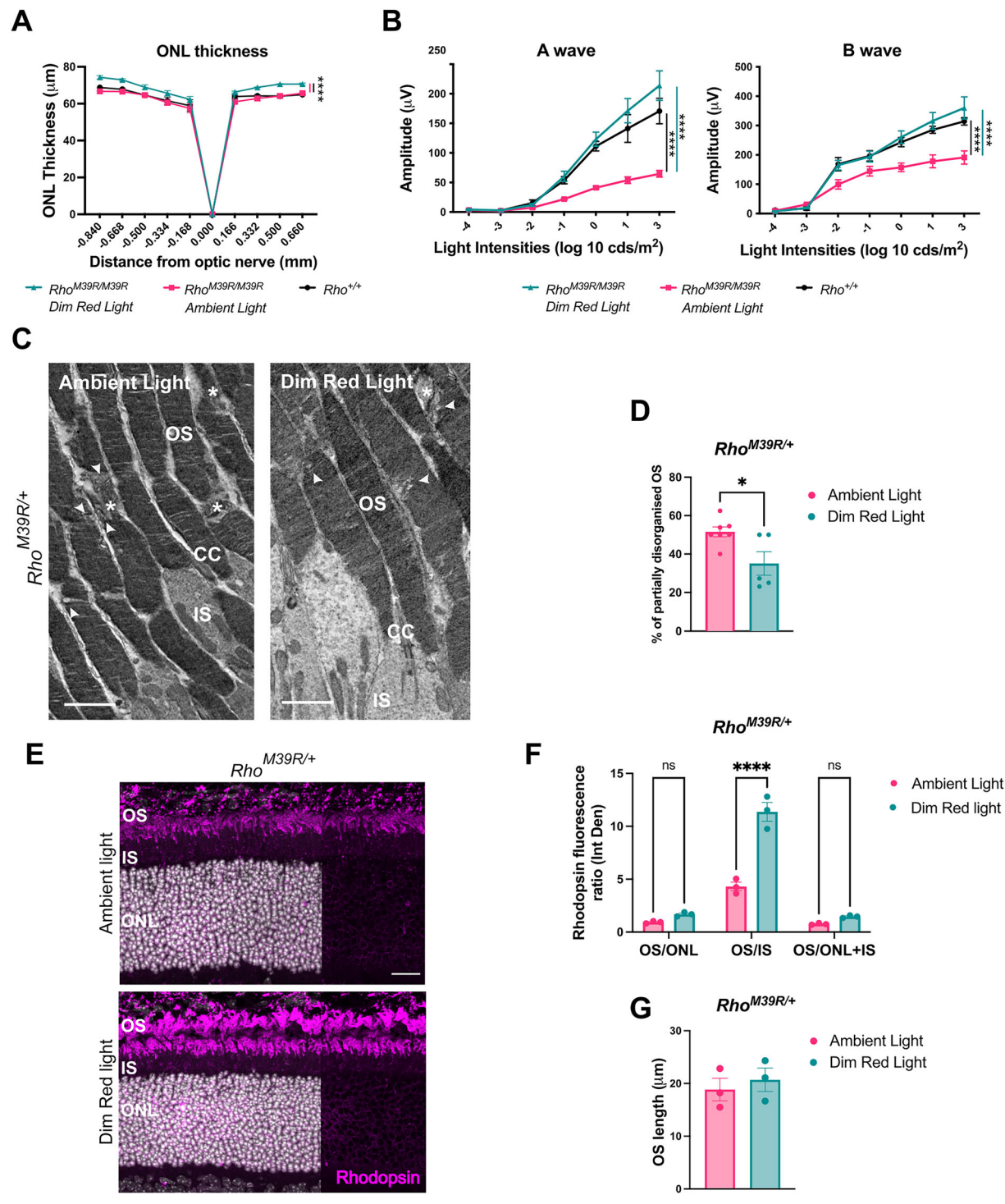


Fig. 4 The role of dim red light in $Rho^{M39R/+}$ KI mice. $Rho^{M39R/+}$ KI mice were reared in red cages under dim red light until 3 weeks of age. **A** The ONL thickness of $Rho^{M39R/+}$ KI (N=5) reared in dim red light was compared to the ONL thickness of respectively $Rho^{+/+}$ and $Rho^{M39R/+}$ KI mice reared in ambient light. The measurements were taken by OCT. Mean \pm SEM. Two-way ANOVA. Tukey's multiple comparisons test between groups. **B** Scotopic A and B waves were recorded for the same set of animals: $Rho^{M39R/+}$ KI in dim red light and ambient light; and $Rho^{+/+}$ KI mice reared in ambient light. Mean \pm SEM. Two-way ANOVA. Tukey's multiple comparisons test between groups. (*****p < 0.0001). **C** The TEM images showed the ultrastructure of $Rho^{M39R/+}$ KI mice reared in dim red light and ambient light. Stars identify transversally orientated discs, while arrowheads indicate vesicular structures. Scale bar $= 2 \mu m$. OS = 0 Outer Segment, CC = 0 connecting cilium, IS = 0 Inner Segment. **D** The % of partially disorganised RO (with transversally orientated discs and/or vesicular structures) was plotted. Mean \pm SEM. Mann-Whitney test (*p < 0.05). 5–7 images from two independent animals. **E** Eyes from mice in red cages were enucleated after ERG and OCT and fixed in 4% PFA. Eye cryosections were stained with anti-rhodopin-4D2 antibody (in magenta) Scale bar $= 20 \mu m$. **F** The integrated density of rhodopsin signal was measured in the different layers of the retina by using Fuji and plotted as a ratio. Mean \pm SEM. Two-way ANOVA. Sidak's multiple comparisons test (*p < 0.05, **p < 0.01). N = 3. **G** The length of the OS was measured by using Fuji. Mean \pm SEM. Two-tailed unpaired t-test. N = 3. OS = 0 Outer Segment, CC = 0 connecting cilium, IS = 0 Inner Segment, ONL = 0 Outer Nuclear Layer, INL = 0 Inner Nuclear Layer.

involved in the rhodopsin M39R-mediated mechanisms of cell death.

S1P receptor as a pharmacological target for Rhodopsin M39R light-induced degeneration

Sphingolipid signalling pathways can be pharmacologically targeted. Several small molecules targeting the S1P receptors, such as Fingolimod/FTY720, are effective in preserving cell viability in pathological conditions [26, 27]. To investigate if S1pr2 and S1pr3 play a critical role in light-induced photoreceptor degeneration in our model, we treated both Rho^{M39R/+} and *Rho*^{M39R/M39R} mice with FTY720 to modulate S1P receptors. Previous reports on light-induced retinal stress treated animals just before the light exposure [22, 28]. Therefore, we injected the mice with 10 mg of FTY720/kg body 30 min prior to induction of light damage with ERG. *Rho*^{M39R/+} mice were injected before each ERG, and each ERG was repeated every week for 4 rounds (until day 21), starting with mice at 4 weeks of age (Fig. 6B). The last ERG was performed to investigate potential changes in retina activity following the treatment (Supplementary Fig. 10A). Rho^{M39R/+} were treated with FTY720, vehicle or left untreated. The ONL thickness was measured at each time point in both treated and untreated mice to monitor the degree of degeneration (Supplementary Fig. 9A, B). After repeated ERG, the mice treated with FTY720 had a thicker ONL than the untreated and vehicle-treated $Rho^{M39R/+}$ mice (Fig. 6C); however, no changes were detected in ERG responses (Supplementary Fig. 10A). The ONL thickness in FTY720-treated mice decreased a little compared to day 0, but the rate of degeneration was much slower than untreated and vehicle-treated animals (Supplementary Fig. 9B). The degeneration in untreated and vehicle-treated retinae was observed predominantly in the superior retina. Measurement of the number of photoreceptors in fixed and cryosectioned Rho^{M39R/+} retinae confirmed the improved photoreceptor survival following treatment (Supplementary Fig. 10B). In addition, in untreated and vehicle-treated animals at day 21, Müller cells were activated and expressed GFAP; whereas, this reactivity was reduced in FTY720treated retinae (Fig. 6D, E). The GFAP-positive area occupied by reactive Müller cells in the ONL, the outer plexiform layer (OPL), and inner nuclei layer (INL) was significantly decreased in the superior retina of FTY720-treated retinae compared to untreated and vehicle-treated retinae (Fig. 6E). A smaller reduction was also observed in the inferior retina, even if not statistically significant (Fig. 6E). Rho^{+/+} mice were also injected with FTY720 or vehicle to confirm the drug safety. No changes in the ONL thickness or retina activity were observed (Supplementary Figs. 11A–C). Four week old *Rho^{M39R/M39R}* mice were injected with FTY720

Four week old *Rho^{M39R/M39R}* mice were injected with FTY720 before a single ERG, while OCT measurement was performed at day 0 and after 2 days (Fig. 7A). FTY720-treated mice had less retinal degeneration than untreated and vehicle-injected mice (Fig. 7B). Similar to the *Rho^{M39R/+}* mice, the administration of FTY720 did not completely prevent retinal degeneration (Supplementary Fig. 12B). Nevertheless, the FTY720 treatment prior to light exposure significantly reduced the amount of photoreceptor loss (Fig. 7C, D). Interestingly, Müller glia activation did not differ in FTY720-treated retina compared to untreated and vehicle-treated (Supplementary Fig. 13A, B).

These data suggest that S1PRs play a critical role in the mechanism of light-induced photoreceptor cell death mediated by rhodopsin M39R. Therefore, blocking S1PRs activity could delay retinal degeneration and reduce light-dependent *Rho*^{M39R} phenotypes.

DISCUSSION

In this study, we developed a new mouse model for sector RP that replicates key features of the disease. The Rho^{M39R/+} mouse model exhibits mild inferior retinal degeneration by 5 months of age,

replicating both the region-specificity and the late-onset of sector RP [14, 15]. The inferior retina is more likely to be affected by light for anatomical and environmental reasons. In particular, the lens of the eye inverts the image, and if light comes from upper visual field, it falls on the inferior retina. Most light comes from above, for example, the sun or bright ceiling lights; therefore, there is greater exposure of the inferior retina to bright light. These are believed to be the main reasons that patients with sector RP and the RHO^{M39R} variant show initial degeneration in the inferior and inferior-nasal retina. Our data confirmed the critical role of both bright and ambient light in exacerbating the phenotype and accelerating retinal degeneration in a sector RP model. In addition, it highlights that even a diagnostic test, such as the ERG, could play a critical role in sector RP progression by inducing further degeneration in the centre of the retina.

C57BL/6J mice are less sensitive to light damage than other strains of mice and particularly albino mice [29]; however, C57BL/6J mice carrying the murine *Rho*^{M39R} variant showed extreme light sensitivity and retinal degeneration induced by short exposure to bright light via ERG. Some other rhodopsin models show a similar sensitivity to light. For example, short exposure to bright light or fundus photography can cause light-induced toxicity in transgenic (tg) mice carrying the hT17M mouse [30, 31]. T17M, together with T4K and T4R, are rhodopsin mutations that inhibit the N-terminal glycosylation of the protein and are associated with sector RP [32–34]. A few *Rho*^{T17M} KI models have been recently generated, but their sensitivity to light was not studied [35, 36]. The role of T4K has been predominantly studied in *X. laevis*, while T4R has been investigated in a naturally occurring dog model. Both models confirmed the critical role of light in rhodopsin T4K and T4R-induced retinal degeneration [32–34, 37].

Other rhodopsin amino acid substitutions, such as Y102H and I307N, can lead to light-dependent degeneration after short exposure to bright light (12,000 lux per 5 min) in mutagenised C57BL/6J mouse lines (Tvrm1 and Tvrm4 mice, respectively) [38, 39]. However, these amino acid changes have not been associated with sector RP in patients. Furthermore, rhodopsin Y102H and I307N did not affect the activity of the retina from early stages, or lead to ONL length reduction in mice up to 12 months of age prior to light damage [38]. Rhodopsin P23H is also associated with sector RP, and its sensitivity to light damage has been investigated in several models, including rodents, *X. laevis*, and *Drosophila* [30, 40–45]. Although *Rho* hP23H tg mice are also sensitive to short exposure of bright light, these mice exhibit lower sensitivity compared to *Rho* hT17M tg mice [30]. In contrast, rhodopsin P23H transgenic rats, which are albino, primarily experience light-induced toxicity following prolonged exposure to bright light [41].

In the T4K *X. laevis* transgenic model, reduced RPE65 activity can rescue the light-induced toxicity [37]. In contrast, in Y102H and I307N mice and P23H *X. laevis*, the ablation of RPE65 exacerbated the phenotype [37, 38]. The Moritz lab proposed two mechanisms of light-induced degeneration in sector RP: "chromophore-exacerbated" (T4K-like) and "chromophore-mitigated" (P23H-like). The two divergent phenotypes within *RHO* variants associated with sector RP could also depend on the different biological classification: class 4 for T4K and class 2 for P23H, respectively [5]. *RHO* M39R is a class 4 mutation and, similarly to canine rhodopsin T4R, shows a faster decay of meta-rhodopsin II, and thermal instability [15, 34]. Further investigations will be necessary to elucidate the role of RPE65 and 11-*cis*-retinal in M39R mice.

The *Rho^{M39R}* model provides deeper insights into the role of rhodopsin class 4 variants in OS stability and retina degeneration. Class 4 variants are hypothesised to cause instability of the OS. The data show that rhodopsin traffics to the OS in both *Rho^{M39R/+}* and *Rho^{M39R/M39R}*, and the OS has structural alterations. *Rho^{M39R/+}* OS show frequent disorganised areas together with a thinner diameter, while rhodopsin levels are comparable to the levels



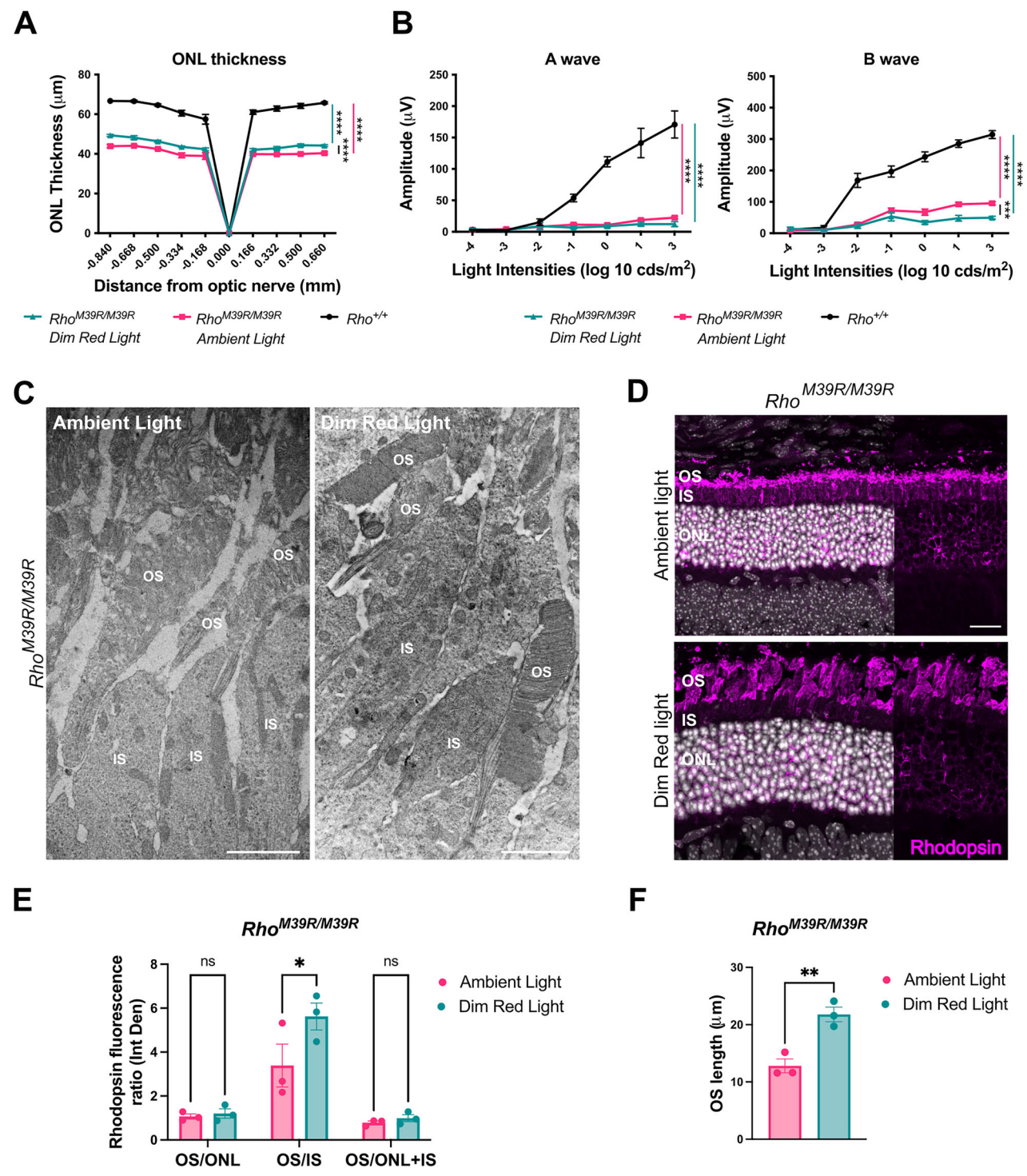


Fig. 5 The role of dim red light in $Rho^{M39R/M39R}$ KI mice. $Rho^{M39R/M39R}$ KI mice were reared in red cages under dim red light until 3 weeks of age. A The ONL thickness of $Rho^{M39R/M39R}$ KI mice (N = 5) reared in dim red light was compared to the ONL thickness of mice reared in ambient light. The ONL thickness of $Rho^{+/+}$ mice reared in ambient light was also plotted. The measurements were taken by OCT. Mean \pm SEM. Two-way ANOVA. Tukey's multiple comparisons test between groups. (*****p < 0.0001). B Scotopic A and B wave of $Rho^{M39R/M39R}$ KI in dim red light and ambient light, and $Rho^{+/+}$ mice reared in ambient light was also reported. Mean \pm SEM. Two-way ANOVA. Tukey's multiple comparisons test between groups. C The ultrastructure of $Rho^{M39R/M39R}$ KI mice reared in dim red light and ambient light was analysed by TEM. Scale bar = 2 μ m. OS = Outer Segment, IS = Inner Segment. D Eyes from mice in red cages were enucleated after ERG and OCT and fixed in 4% PFA. Eye cryosections were stained with anti-rhodopin-4D2 antibody (in magenta). E The integrated density of rhodopsin signal was measured in the different layers of the retina by using Fuji and plotted as a ratio. Mean \pm SEM. Two-way ANOVA. Sidak's multiple comparisons test (*p < 0.05, **p < 0.01). N = 3. F The length of the OS was measured by using Fuji. Mean \pm SEM. Unpaired t-test (**p < 0.01). OS = Outer Segment, CC = connecting cilium, IS = Inner Segment, ONL = Outer Nuclear Layer, INL = Inner Nuclear Layer.

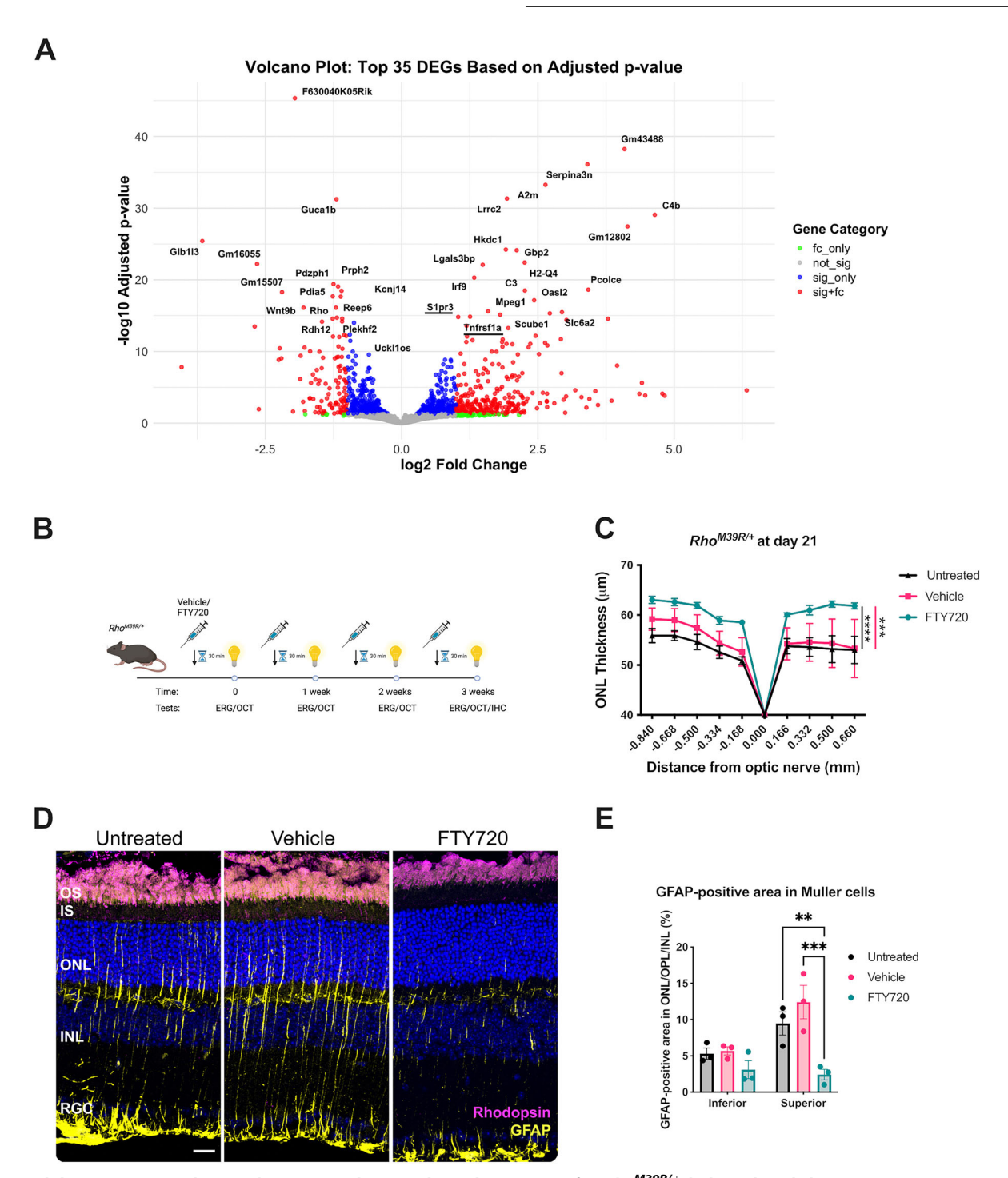


Fig. 6 Modulating S1P signaling pathway as a pharmacological treatment for $Rho^{M39R/+}$ light-induced degeneration. A Transcriptomic analysis by bulk RNA-seq of $Rho^{M39R/M39R}$ KI retinae compared to control mice. The volcano plot shows the top 35 differentially expressed genes by adjusted p value. S1P signalling pathway genes are underlined in red. fc_only = only fold change; not_sign = not significant; sig_only = only significant; sig_fc = significant plus fold change. B $Rho^{M39R/+}$ KI mice were treated with FTY720 at 4 weeks of age. Schematic of the treatment in $Rho^{M39R/+}$ KI mice. The animals were dark-adapted overnight and intraperitoneally injected with 10 mg/kg of FTY720 or vehicle (saline solution) 30 min before performing the light damage assay. The light damage consisted in performing an ERG every week for 4 times in total. Each time, the mice were preinjected with FTY720 or vehicle. C The ONL thickness was measured at day 21, after 4 rounds of ERG. FTY720-treated mice were compared to vehicle-treated and untreated mice. Mean ± SEM. Two-way ANOVA. Tukey's multiple comparisons test between groups. (****p < 0.0001, ***p < 0.0001). Untreated N = 5, vehicle treated N = 7, FTY720 treated N = 6. D At the end of the light damage experiments, mice were culled, and the eyes were encleated to perform further histological investigations. Rodents eyes were fixed in 4% PFA, incubated in 30% sucrose for 1–2 days, embedded in OCT (embedding matrix), cryosectioned and stained with DAPI. IHC of untreated, vehicle or FTY70 treated $Rho^{M39R/+}$ superior retina after light damage. The cryosections were stained with rhodospin-4D2 (in magenta) and anti-GFAP (in yellow). Scale bar = 20 μ m. E The % area occupied by GFAP-positive signal relative to the ONL, OPL, and INL was measured after thresholding GFAP staining in untreated and treated animals. Analysis performed in Fiji. Mean ± SEM. Two-way ANOVA. Tukey's multiple comparisons test between groups. (***p < 0.001), ****p < 0.001), ****p < 0.

measured in *Rho*^{+/+} animals. In heterozygous mice, where 50% of the rhodopsin protein is wild-type RHO, disc formation is similar to the control animals, and the presence of rhodopsin M39R causes only a partial OS dysregulation, with vesicular structures intercalated in transversally oriented discs. In contrast, the OS structure changes completely when only rhodopsin M39R is expressed. The intrinsic instability of rhodopsin M39R [15], in combination with the amino acid change occurring in the first transmembrane domain might affect the formation and stability of the discs and therefore lead to highly disorganised and shorter OS. In addition, transcriptomic analysis performed on *Rho*^{M39R/M39R} mice reveals the downregulation of *Prph2*, a crucial gene involved in OS disc morphogenesis [46–48].

In 3-week-old *Rho^{M39R/M39R}*, the amount of rhodopsin is around 70% lower than in *Rho^{+/+}* mice. There is also a 30–40% reduction in ONL thickness, which might account for some of this decrease, but does not fully account for the decrease in rhodopsin levels. The reasons why rhodopsin levels are reduced by more than photoreceptor cell loss could reflect changes in transcription, protein degradation, or increased OS turnover. In *Rho^{M39R/M39R}* mice, rhodopsin M39R is indeed found in both the ONL and IS. In addition, transcriptomics and immunohistochemistry show increased levels of *Gfap* expression and GFAP-positive Müller glia at 3 weeks of age, respectively (data not shown), confirming retinal degeneration in *Rho^{M39R/M39R}* mice from an early stage.

Bright light exposure led to a further dysregulation of the disc structure in *Rho*^{M39R/+} (TEM data not shown), similar to what was previously reported for other light damage models [49, 50]. After light, *Rho*^{M39R/M39R} OS become smaller and were mainly formed of vesicular structures. In contrast, rearing the animals in dim red light decreased OS instability in both models and reduce retinal degeneration in *Rho*^{M39R/M39R}. In *Rho*^{M39R/M39R}, the absence of light facilitates the formation of proper compact discs and improves rhodopsin localisation at the OS, reducing the accumulation of the protein in the IS.

Moreover, even though rhodopsin M39R localised at the OS in the presence and absence of WT rhodopsin, there was reduced photoreceptor activity. Rhodopsin M39R, as previously described, can activate phototransduction but with a faster meta-rhodopsin II decay [15]. However, the scotopic A wave recorded in Rho^{M39R/+} at 3 weeks of age was significantly lower than in $Rho^{+/+}$ mice. In contrast, rearing animals in dim red light rescued the activity in $Rho^{M39R/+}$, similar to what has been previously observed in $Rho^{P23H/+}$ KI mice [43]. We hypothesise that after ambient light exposure, rhodopsin M39R might be highly phosphorylated and/ or not properly dephosphorylated, and that the higher phosphorylation level could lead to increased recovery time and reduced sensitivity to light [51, 52]. In dim red light, rhodopsin M39R is unphosphorylated, and therefore it can respond normally to the initial light exposure. Further analysis would be needed to test this hypothesis. However, in *Rho^{M39R/M39R}* mice, the scotopic A wave, which is further impaired compared to *Rho^{M39R/+}* mice, cannot be rescued in dim red light. Further investigation will be requested to understand if this is due to constitutive instability of the protein and consequently of the OS, despite a measured improvement.

Transcriptomic analysis was performed on the Rho^{M39R/M39R}, as this model exhibits retinal degeneration under ambient light. These data provided insights into the gene expression changes in a sector RP model in ambient light. Changes in genes of the S1P signalling pathway were identified. The S1P signalling pathway and de novo ceramide synthesis are among the pathways that show dysregulation in light damage models [53]. In response to light damage, the levels of ceramides and ceramide-related metabolic genes increase in albino rats and Tvrm4 mice [22, 39]. In addition, TNF Receptors such as Tnfrsf1a respond to changes in sphingolipid levels and have been associated with mechanisms of light-induced toxicity [22–24, 28]. Moreover, bright light exposure in albino rodents has been shown to elevate S1P levels, along with

the expression of S1P kinases (SphKs) and S1P receptors (S1PRs) [22–24]. Nevertheless, mice lacking *SphK2* were still photosensitive to light damage [54]. S1P is important for cell proliferation and survival [55]. In the retina, it plays a key role in maintaining outer limiting membrane (OLM) stability and regulating cytoskeletal rearrangements in Müller cells [56].

S1pr3 and S1pr2 transcripts expression was increased in $Rho^{M39R/M39R}$ mice compared to $Rho^{+/+}$ mice. In albino rats, immunohistochemistry showed that both S1P receptors are expressed in bipolar cells, but only S1pr3 localised in photoreceptors (in both the IS and ONL) [23]. A more recent study, however, showed that S1P receptors are mainly expressed in Müller cells in chick retina and that the S1PR modulator FTY720 reduced Müller glia-derived progenitor cells in response to NMDA treatment, suggesting Müller cells could be a major site of S1PR function [57]. scRNAseq data from wildtype C57BL/6J confirmed that Müller cells appear to express the highest levels of S1pr2 and S1pr3 in mouse retina [25]. Further work will be needed to determine which cells upregulate S1PR expression in M39R models and if this is further exacerbated by light, as well as which S1PRs might be involved in the pathogenesis of light-induced degeneration in M39R rhodopsin RP.

FTY720 can reduce the light-induced toxicity from bright light in albino rats [22]. FTY720 is an approved treatment for Multiple Sclerosis that acts on the central nervous system by modulating inflammation and by improving neuronal function [58–60]. Our data in *Rho^{M39/+}* mice confirm the crucial role of FTY720 in preventing light damage by both reducing photoreceptor loss and activation of Müller cells. In *Rho^{M39R/M39R}* mice, FTY720 treatment significantly improved photoreceptor survival but did not alter the inflammatory response. In these homozygous mice, Müller cells were already activated and microglia were recruited to the ONL by 3 weeks of age under cyclic ambient light conditions, even before light-induced damage occurred. Retinal activity did not improve with FTY720 treatment; therefore, our findings suggest that FTY720 may function by downregulating cell death signalling downstream of the rhodopsin M39R response to light, possibly by acting on S1PR in Müller cells.

In conclusion, our data provide new insights into sector RP retinal degeneration and suggest two potential strategies to mitigate light-induced toxicity: reducing light exposure and implementing a therapeutic approach targeting the sphingolipid signalling pathways.

MATERIALS AND METHODS

Animal care

All animal procedures were carried out in accordance with UK Home Office regulations under the Animals (Scientific Procedures) Act of 1986 and were approved by the ethics committee of the UCL Institute of Ophthalmology, London, UK. The Rho^{M39R} line was generated by CRISPR-Cas9 HDR technology on C57BL/6 J mouse strain. A specific gRNA (Supplementary Table 1) was used in combination with a donor template containing a change in the spCas9 PAM site (CCA > CTC) and introducing the Met to Arg (ATG > AGG) mutation. $Rho^{+/+}$ C57BL/6J mice were used as controls. Except for light manipulation experiments, animals were kept on a 12-h light (20–100 lux) and 12-h dark (<10 lux) cycle, with free access to food and water.

Drug administration

Mice in dim red light were injected intraperitoneally with vehicle (saline solution) or FTY720 (Bio-techne, Tocris, 1 mg/ml in saline solution). The injections were performed 30 min prior to ERG. FTY720 was injected at a concentration of 10 mg/kg as already described [22]. To perform OCT/ERG, mice were anesthetized using Ketamine (Dechra, 1.2 mg/kg) and Medetomidine/Domitor (Orion Pharma, 1 mg/kg), and recovered for longitudinal experiments by administrating Atipamezole/Antisedan (Orion Pharma, 1.3 mg/kg).

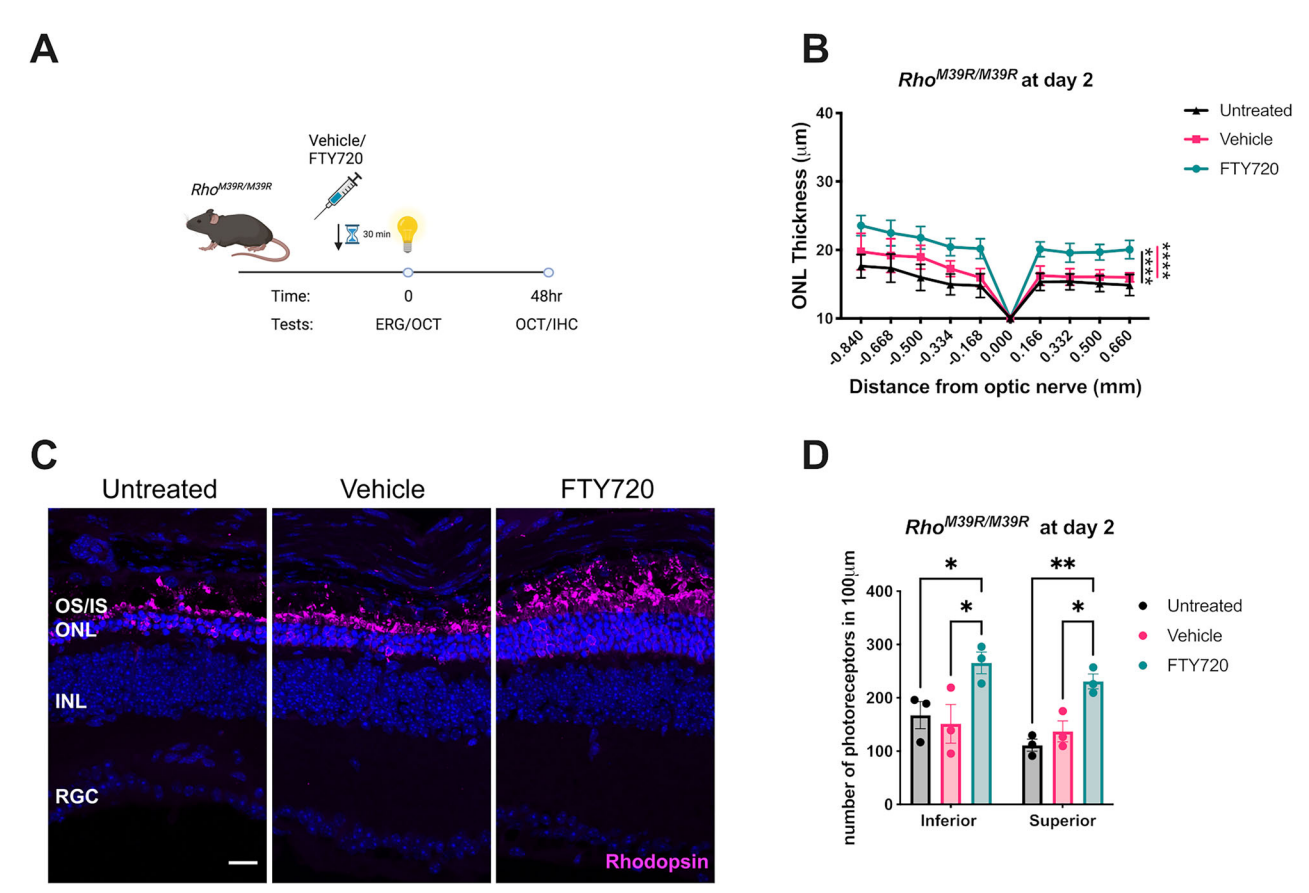


Fig. 7 Modulating S1P signaling pathway as a pharmacological treatment for $Rho^{M39R/M39R}$ light-induced degeneration. A $Rho^{M39R/M39R}$ KI mice were treated with FTY720 at 4 weeks of age. Schematic of the FTY20 treatment in $Rho^{M39R/M39R}$ KI mice. Mice were dark-adapted and injected with FTY720 (10 mg/kg) 30 min prior to the light damage assay. The ERG was performed once to induce a faster degeneration. The OCT was performed at both day 0 and day 2, after 48 h from the single ERG. B The ONL thickness was measured at day 2, after a single ERG. FTY720-treated $Rho^{M39R/M39R}$ KI mice were compared to vehicle-treated and untreated mice. Mean ± SEM. Two-way ANOVA. Tukey's multiple comparisons test between groups. (*****p < 0.0001, ****p < 0.001). Untreated N = 6, vehicle and FTY720 treated N = 5. C IHC of untreated, vehicle or FTY70 treated $Rho^{M39R/M39R}$ superior retina after light damage. The cryosections were stained with rhodospin-4D2 (in magenta). Scale bar = 20 μm. D The number of photoreceptors in the ONL was measured at 200–400 μm from the optic nerve in the inferior and superior retina. The analysis was performed on images of the central retina acquired with a microscope EVOS FL auto 2. The area of 10–20 nuclei per retina was measured and divided to total area of the ONL to calculate the total number of nuclei. The number of photoreceptors in 100 μm per treated/untreated animal was plotted. Mean ± SEM. Two-way ANOVA. Tukey's multiple comparisons test between groups. (*p < 0.05, *** p < 0.01). N = 3.

Electroretinogram (ERG)

Mice were dark-adapted overnight and anaesthetised before starting the procedure. Pupils were dilated with topical application of 1% tropicamide (Bausch and Lomb, UK). Electroretinography (ERG) was conducted using a Celeris machine (Diagnosys LLC, UK) under dim red light conditions. Flash stimuli (0.1 ms to 30 ms duration, repetition rate 0.2 Hz) were delivered by the stimulator (log intensity —4 to +3) to assess the scotopic activity of the retina. A and B wave responses were recorded, and the data were exported and analysed by Excel (Microsoft) and Prism/GraphPad (Dotmatics).

Optical coherence tomography (OCT)

Retinae of anaesthetised animals were imaged using the Bioptigen Envis R2300 Spectral-domain ophthalmic imaging system (SDOIS). Images were captured using the InVivoVue Clinic while administrating topical Systane Ultra (Alcon) lubricant eye drops application to prevent cornea dryness. Manual segmentation of the retinal layers was performed using the Bioptigen InVivoVue Diver 2.0 software to measure the outer nuclear layer (ONL) thickness. Exported results were analysed by Excel (Microsoft) and Prism/GraphPad (Dotmatics).

Transmission electron microscopy (TEM)

Mouse eyes were isolated and were immediately fixed in Karnovsky's fixative overnight at 4 °C. The day after, after rinsing with 0.1 M sodium cacodylate-HCl buffer (pH 7.4), the samples were post-fixed in 1%

aqueous osmium tetroxide for 2 h at room temperature, then dehydrated by passage through ascending alcohols (1 \times 30%, 50%, 70%, 90% and 2 \times 100%), and two changes of 100% propylene oxide. Samples were infiltrated with 100% resin over 4–6 h, and then embedded in fresh resin, which was then cured by 48-h incubation at 60 °C. Ultra-thin sections (85 nm) were collected on 150 hex copper TEM grids and were contrasted with Reynold's lead citrate for 5 min at room temperature. Prepared sections were then imaged at TEM JEOL 1400plus operating at 80 kV. Images were captured using a Deben NanoSprint12S camera using the Advanced Microscopy Techniques (AMT) Imaging Software.

Protein extraction and Western blot

Mouse retinal tissue was lysed in 200 μ L RIPA buffer (1% sodium deoxycholate, 150 mM NaCl, 1% NP-40, 0.1% SDS, 50 mM Tris-HCl, pH = 7.5) containing 2% (v/v) protease inhibitor cocktail (PIC; Sigma) and 1% (v/v) Phosphatase inhibitor cocktail (PHC, Sigma) on ice. Tissue was further disrupted by a brief sonication of 20 s at 0.1 watts using an Ultrasonic Liquid Processor XL-2000 (Misonix Incorporated), and lysates were then centrifuged at $13,000 \times g$ for 10 min at 4 °C for the removal of cellular and DNA debris. Supernatant was then collected, and protein quantification was completed using the Pierce Bicinchoninic acid (BCA) Protein Assay (Thermofisher) following the manufacturers microplate procedure. Absorbance at 562 nm of standards and samples was quantified using a spectrophotometer (Safire, Tecan).

Protein extraction was performed in RIPA Buffer starting from dissected mouse retina. Following protein quantification, 3-5 µg of protein of each sample was mixed with Sample buffer 4X (0.025% bromophenol blue, 10% β-mercaptoethanol, 20% glycerol, 5% SDS, 125 mM Tris-HCl, pH = 7). The tissue lysates that were blotted with rhodopsin antibodies remained unheated. The samples were loaded in 10% acrylamide gels and resolved by SDS-polyacrylamide gel electrophoresis (SDS-PAGE). Protein was then transferred to nitrocellulose membranes via wet transfer using Transfer buffer (25 mM Tris, pH = 8.3, 192 mM glycine, 0.01% SDS, and 20%methanol). Membranes were blocked with 5% (w/v) powdered milk (Marvel) in PBS containing 0.1% TWEEN-20 (PBS-T, Sigma). Blots were incubated with primary antibodies (Supplementary Table 4), diluted in 2.5-3% milk PBS-T, overnight at 4 °C with shaking. The next day, blots were washed three times in PBS-T, followed by a 2-h incubation with HRP-conjugated secondary antibody, diluted in 2.5% (w/v) milk PBS-T. Following secondary incubation, membranes were washed with PBS-T three times and protein detected using Luminata Crescendo or Forte western HRP substrate (Millipore) and imaged with ImageLab on a BioRad ChemiDoc XRS+.

Immunohistochemistry (IHC)

Enucleated mouse eyes were fixed in a 4% PFA solution overnight, washed with PBS, and incubated in 30% sucrose for 24-48 h, then snap frozen in OCT Embedding matrix (Cell Path) and cryosectioned at 10 µm. Slides were washed 3 times with PBS, incubated in Blocking Buffer (BB) (10% serum, 3% BSA in 0.1% Triton-X PBS), incubated in primary antibody solution (Supplementary Table 2), washed 3 times, and finally incubated in secondary antibody solution (Supplementary Table 2). Each incubation was 1 h long at room temperature (RT). A final incubation with 4',6diamidino-2-phenylindole (DAPI) in water/PBS for 5 min at RT was performed prior to mounting the slides in fluorescence mounting media (DAKO). Images were acquired using a LSM700 laser-scanning confocal microscope (Carl Zeiss) or Stellaris 8 (Leica) and processed using Image J (National Institute of Health, Bethesda, MD, USA) and Illustrator (Adobe).

Light damage assay

Light damage was induced by repeated ERG every week for 4 weeks, starting from mice at 3 or 4 weeks of age. Maximum light intensity was 30,000 lux for 2 flashes.

RNA extraction and RNA-sequencing (RNA-seq)Total RNA was extracted from $Rho^{+/+}$ and $Rho^{M39R/M39R}$ at 3 weeks as previously described [61]. Bulk RNAseq was performed by Azenta. RNA-seq data were analysed using the R statistical environment (v4.5.0). Raw read counts were processed and normalized with the DESeq2 package (v1.48.0, Bioconductor), applying default settings including size factor normalization and dispersion estimation. Genes with low counts (<10 reads) across all samples were filtered prior to differential expression testing. Differentially expressed genes (DEGs) were identified using the DESeq2 Wald test, with significance thresholds set at adjusted p-value < 0.05 following Benjamini-Hochberg correction for multiple testing. Volcano plots were generated using the ggplot2 package (v3.5.2) and ggrepel (v0.9.6) for label repelling, with genes color-coded according to significance thresholds. Heatmaps were constructed using the pheatmap package (v1.0.12). Variance-stabilizing transformation (VST) was applied to normalized counts using DESeq2, and average expression values per condition were calculated. Expression values were centered by subtracting the global mean across all genes and conditions. KEGG pathway enrichment analysis was conducted using the clusterProfiler package (v4.16.0) after converting gene symbols to Entrez IDs via org.Mm.eg.db (v3.21.0). Enrichment was performed against the Mus musculus KEGG database (organism = "mmu"). The top 20 enriched KEGG pathways were visualized using the enrichplot

The data discussed in this publication have been deposited in NCBI's Gene Expression Omnibus [62] and are accessible through GEO Series accession number GSE304732 (https://www.ncbi.nlm.nih.gov/geo/guery/ acc.cgi?acc=GSE304732).

Statistics

Experiments were conducted using both sexes in equal proportion. Sample sizes were not determined using a formal power analysis. The number of animals was selected based on prior experience, standard practice in similar studies, and ethical considerations to balance statistical robustness with animal welfare. Blinding was not implemented

due to the nature of the experimental procedures, which required investigator involvement throughout the study. However, objective and quantitative outcome measures were used to mitigate potential bias. Normality and homogeneity of variance (heteroscedasticity) were assessed to determine the appropriate statistical tests. An unpaired Student's t-test was used for comparisons between two groups when analysing a single independent variable, and assumptions of normality were met. When normality was not satisfied or sample sizes were small, the non-parametric Mann-Whitney U test was applied. One-way ANOVA was used for comparisons involving more than two groups with a single independent variable, while two-way ANOVA was employed to evaluate the effects of two independent variables. Specific details, including post hoc tests where applicable, are provided in the figure legends. All analyses were performed using GraphPad Prism, version 10, and statistical significance was set at p < 0.05.

REFERENCES

- 1. Hartong DT, Berson EL, Dryja TP. Retinitis pigmentosa. Lancet. 2006;368:1795–809.
- 2. Berson EL, Rosner B, Weigel-DiFranco C, Dryja TP, Sandberg MA. Disease progression in patients with dominant retinitis pigmentosa and rhodopsin mutations. Investig Ophthalmol Vis Sci. 2002;43:3027-36.
- Guarascio R, Cheetham ME. Light as a mediator of acute and chronic retina degeneration. Adv Exp Med Biol. 2025;1468:247-51.
- 4. Dryja TP, McGee TL, Reichel E, Hahn LB, Cowley GS, Yandell DW, et al. A point mutation of the rhodopsin gene in one form of retinitis pigmentosa. Nature. 1990:343:364-6
- 5. Athanasiou D, Aguila M, Bellingham J, Li W, McCulley C, Reeves PJ, et al. The molecular and cellular basis of rhodopsin retinitis pigmentosa reveals potential strategies for therapy. Prog Retin Eye Res. 2018;62:1-23.
- 6. Palczewski K. G protein-coupled receptor rhodopsin. Annu Rev Biochem. 2006;75:743-67.
- 7. Travis GH, Golczak M, Moise AR, Palczewski K. Diseases caused by defects in the visual cycle: retinoids as potential therapeutic agents. Annu Rev Pharm Toxicol. 2007:47:469-512.
- 8. Lin JH, Li H, Yasumura D, Cohen HR, Zhang C, Panning B, et al. IRE1 signaling affects cell fate during the unfolded protein response. Science. 2007:318:944-9
- 9. Athanasiou D, Kosmaoglou M, Kanuga N, Novoselov SS, Paton AW, Paton JC, et al. BiP prevents rod opsin aggregation. Mol Biol Cell. 2012;23:3522-31.
- 10. Sullivan LS, Bowne SJ, Reeves MJ, Blain D, Goetz K, Ndifor V, et al. Prevalence of mutations in eyeGENE probands with a diagnosis of autosomal dominant retinitis pigmentosa. Investig Ophthalmol Vis Sci. 2013;54:6255-61.
- 11. Olsson JE, Gordon JW, Pawlyk BS, Roof D, Hayes A, Molday RS, et al. Transgenic mice with a rhodopsin mutation (Pro23His): a mouse model of autosomal dominant retinitis pigmentosa. Neuron. 1992;9:815-30.
- 12. Pennesi ME, Nishikawa S, Matthes MT, Yasumura D, LaVail MM. The relationship of photoreceptor degeneration to retinal vascular development and loss in mutant rhodopsin transgenic and RCS rats. Exp Eye Res. 2008;87:561-70.
- 13. Sakami S, Maeda T, Bereta G, Okano K, Golczak M, Sumaroka A, et al. Probing mechanisms of photoreceptor degeneration in a new mouse model of the common form of autosomal dominant retinitis pigmentosa due to P23H opsin mutations. J Biol Chem. 2011;286:10551-67.
- 14. Georgiou M, Grewal PS, Narayan A, Alser M, Ali N, Fujinami K, et al. Sector retinitis pigmentosa; extending the molecular genetics basis and elucidating the natural history. Am J Ophthalmol. 2021;221:299-310.
- 15. Ramon E, Cordomí A, Aguilà M, Srinivasan S, Dong X, Moore AT, et al. Differential light-induced responses in sectorial inherited retinal degeneration. J Biol Chem. 2014;289:35918-28.
- 16. Modzelewski AJ, Chen S, Willis BJ, Lloyd KCK, Wood JA, He L. Efficient mouse genome engineering by CRISPR-EZ technology. Nat Protoc. 2018;13:1253-74.
- 17. Sakami S, Kolesnikov AV, Kefalov VJ, Palczewski K. P23H opsin knock-in mice reveal a novel step in retinal rod disc morphogenesis. Hum Mol Genet. 2014;23:1723-41.
- 18. Liang Y, Fotiadis D, Maeda T, Maeda A, Modzelewska A, Filipek S, et al. Rhodopsin signaling and organization in heterozygote rhodopsin knockout mice. J Biol Chem. 2004;279:48189-96.
- 19. Rakshit T, Park PS. Impact of reduced rhodopsin expression on the structure of rod outer segment disc membranes. Biochemistry. 2015;54:2885-94.
- 20. Peirson SN, Brown LA, Pothecary CA, Benson LA, Fisk AS. Light and the laboratory mouse. J Neurosci Methods. 2018;300:26-36.
- 21. Hait NC, Maiti A. The role of sphingosine-1-phosphate and ceramide-1-phosphate in inflammation and cancer. Mediat Inflamm. 2017;2017:4806541.
- 22. Chen H, Tran JA, Eckerd A, Huynh TP, Elliott MH, Brush RS, et al. Inhibition of de novo ceramide biosynthesis by FTY720 protects rat retina from light-induced degeneration. J Lipid Res. 2013;54:1616-29.

- Porter H, Qi H, Prabhu N, Grambergs R, McRae J, Hopiavuori B, et al. Characterizing sphingosine kinases and sphingosine 1-phosphate receptors in the mammalian eye and retina. Int J Mol Sci. 2018;19:3885.
- 24. Terao R, Honjo M, Ueta T, Obinata H, Izumi T, Kurano M, et al. Light stress-induced increase of sphingosine 1-phosphate in photoreceptors and its relevance to retinal degeneration. Int J Mol Sci. 2019;20:3670.
- 25. Li J, Choi J, Cheng X, Ma J, Pema S, Sanes JR, et al. Comprehensive single-cell atlas of the mouse retina. iScience. 2024;27:109916.
- González-Fernández B, Sánchez DI, González-Gallego J, Tuñón MJ. Sphingosine 1-phosphate signaling as a target in hepatic fibrosis therapy. Front Pharm. 2017;8:579
- 27. Stiles M, Qi H, Sun E, Tan J, Porter H, Allegood J, et al. Sphingolipid profile alters in retinal dystrophic P23H-1 rats and systemic FTY720 can delay retinal degeneration. J Lipid Res. 2016;57:818–31.
- Luu JC, Saadane A, Leinonen H, Choi EH, Gao F, Lewandowski D, et al. Stress resilience-enhancing drugs preserve tissue structure and function in degenerating retina via phosphodiesterase inhibition. Proc Natl Acad Sci USA. 2023;120:e2221045120.
- LaVail MM, Gorrin GM, Repaci MA, Thomas LA, Ginsberg HM. Genetic regulation of light damage to photoreceptors. Investig Ophthalmol Vis Sci. 1987;28:1043–8.
- White DA, Hauswirth WW, Kaushal S, Lewin AS. Increased sensitivity to lightinduced damage in a mouse model of autosomal dominant retinal disease. Investig Ophthalmol Vis Sci. 2007;48:1942–51.
- Krebs MP, White DA, Kaushal S. Biphasic photoreceptor degeneration induced by light in a T17M rhodopsin mouse model of cone bystander damage. Investig Ophthalmol Vis Sci. 2009;50:2956–65.
- Tam BM, Moritz OL. The role of rhodopsin glycosylation in protein folding, trafficking, and light-sensitive retinal degeneration. J Neurosci. 2009;29:15145–54.
- Cideciyan AV, Jacobson SG, Aleman TS, Gu D, Pearce-Kelling SE, Sumaroka A, et al. In vivo dynamics of retinal injury and repair in the rhodopsin mutant dog model of human retinitis pigmentosa. Proc Natl Acad Sci USA. 2005;102:5233–8.
- Zhu L, Jang GF, Jastrzebska B, Filipek S, Pearce-Kelling SE, Aguirre GD, et al. A
 naturally occurring mutation of the opsin gene (T4R) in dogs affects glycosylation
 and stability of the G protein-coupled receptor. J Biol Chem. 2004;279:53828–39.
- 35. He X, Yan T, Song Z, Xiang L, Xiang J, Yang Y, et al. Correcting a patient-specific Rhodopsin mutation with adenine base editor in a mouse model. Mol Ther. 2025;33:3101–13.
- Liu X, Qiao J, Jia R, Zhang F, Meng X, Li Y, et al. Allele-specific gene-editing approach for vision loss restoration in RHO-associated retinitis pigmentosa. eLife. 2023:12:eR4065
- 37. Tam BM, Paloma B, Chiu CN, Moritz OL. Synchronized photoactivation of T4K rhodopsin causes a chromophore-dependent retinal degeneration that is moderated by interaction with phototransduction cascade components. J Neurosci. 2024:44:e0453242024.
- 38. Budzynski E, Gross AK, McAlear SD, Peachey NS, Shukla M, He F, et al. Mutations of the opsin gene (Y102H and I307N) lead to light-induced degeneration of photoreceptors and constitutive activation of phototransduction in mice. J Biol Chem. 2010;285:14521–33.
- Piano I, D'Antongiovanni V, Novelli E, Biagioni M, Dei Cas M, Paroni RC, et al. Myriocin effect on Tvrm4 retina, an autosomal dominant pattern of retinitis pigmentosa. Front Neurosci. 2020;14:372.
- Galy A, Roux MJ, Sahel JA, Léveillard T, Giangrande A. Rhodopsin maturation defects induce photoreceptor death by apoptosis: a fly model for Rhodopsin-Pro23His human retinitis pigmentosa. Hum Mol Genet. 2005;14:2547–57.
- Organisciak DT, Darrow RM, Barsalou L, Kutty RK, Wiggert B. Susceptibility to retinal light damage in transgenic rats with rhodopsin mutations. Investig Ophthalmol Vis Sci. 2003;44:486–92.
- 42. Scott PA, de Castro JP, DeMarco PJ, Ross JW, Njoka J, Walters E, et al. Progression of Pro23His retinopathy in a miniature swine model of retinitis pigmentosa. Transl Vis Sci Technol. 2017;6:4.
- Orlans HO, Merrill J, Barnard AR, Charbel Issa P, Peirson SN, MacLaren RE. Filtration of short-wavelength light provides therapeutic benefit in retinitis pigmentosa caused by a common rhodopsin mutation. Investig Ophthalmol Vis Sci. 2019;60:2733–42.
- 44. Tam BM, Moritz OL. Dark rearing rescues P23H rhodopsin-induced retinal degeneration in a transgenic Xenopus laevis model of retinitis pigmentosa: a chromophore-dependent mechanism characterized by production of N-terminally truncated mutant rhodopsin. J Neurosci. 2007;27:9043–53.
- Naash ML, Peachey NS, Li ZY, Gryczan CC, Goto Y, Blanks J, et al. Light-induced acceleration of photoreceptor degeneration in transgenic mice expressing mutant rhodopsin. Investig Ophthalmol Vis Sci. 1996;37:775–82.
- Jansen HG, Sanyal S. Development and degeneration of retina in rds mutant mice: electron microscopy. J Comp Neurol. 1984;224:71–84.
- 47. Molday RS, Hicks D, Molday L. Peripherin. A rim-specific membrane protein of rod outer segment discs. Investig Ophthalmol Vis Sci. 1987;28:50–61.

- Lewis TR, Makia MS, Castillo CM, Al-Ubaidi MR, Naash Ml, Arshavsky VY. Photoreceptor disc enclosure is tightly controlled by peripherin-2 oligomerization. J Neurosci. 2021;41:3588–96.
- LaVail MM, Gorrin GM. Protection from light damage by ocular pigmentation: analysis using experimental chimeras and translocation mice. Exp Eye Res. 1987:44:877–89.
- Marsili S, Genini S, Sudharsan R, Gingrich J, Aguirre GD, Beltran WA. Exclusion of the unfolded protein response in light-induced retinal degeneration in the canine T4R RHO model of autosomal dominant retinitis pigmentosa. PLoS ONE. 2015;10:e0115723.
- 51. Zhao X, Palczewski K, Ohguro H. Mechanism of rhodopsin phosphorylation. Biophys Chem. 1995;56:183–8.
- Arshavsky VY. Rhodopsin phosphorylation: from terminating single photon responses to photoreceptor dark adaptation. Trends Neurosci. 2002;25:124–6.
- Simon MV, Basu SK, Qaladize B, Grambergs R, Rotstein NP, Mandal N. Sphingolipids as critical players in retinal physiology and pathology. J Lipid Res. 2021:62:100037
- Qi H, Cole J 2nd, Grambergs RC, Gillenwater JR, Mondal K, Khanam S, et al. Sphingosine kinase 2 phosphorylation of FTY720 is unnecessary for prevention of light-induced retinal damage. Sci Rep. 2019;9:7771.
- Rotstein NP, Miranda GE, Abrahan CE, German OL. Regulating survival and development in the retina: key roles for simple sphingolipids. J Lipid Res. 2010;51:1247–62.
- Wilkerson JL, Stiles MA, Gurley JM, Grambergs RC, Gu X, Elliott MH, et al. Sphingosine kinase-1 is essential for maintaining external/outer limiting membrane and associated adherens junctions in the aging retina. Mol Neurobiol. 2019:56:7188–207.
- Taylor OB, DeGroff N, El-Hodiri HM, Gao C, Fischer AJ. Sphingosine-1-phosphate signaling regulates the ability of Müller glia to become neurogenic, proliferating progenitor-like cells. eLife. 2025;13:RP102151.
- Anastasiadou S, Knöll B. The multiple sclerosis drug fingolimod (FTY720) stimulates neuronal gene expression, axonal growth and regeneration. Exp Neurol. 2016;279:243–60.
- Brinkmann V. FTY720 (fingolimod) in Multiple Sclerosis: therapeutic effects in the immune and the central nervous system. Br J Pharmacol. 2009;158:1173–82.
- Sharma S, Mathur AG, Pradhan S, Singh DB, Gupta S. Fingolimod (FTY720): First approved oral therapy for multiple sclerosis. J Pharmacol Pharmacother. 2011:2:49–51
- Athanasiou D, Afanasyeva TAV, Chai N, Ziaka K, Jovanovic K, Guarascio R, et al. Small molecule treatment alleviates photoreceptor cilia defects in LCA5-deficient human retinal organoids. Acta Neuropathol Commun. 2025;13:26.
- Edgar R, Domrachev M, Lash AE. Gene expression omnibus: NCBI gene expression and hybridization array data repository. Nucleic Acids Res. 2002;30:207–10.

ACKNOWLEDGEMENTS

These authors gratefully acknowledge Hannah Poultney for the help in the animal care, Prof. Robert Molday (University of British Columbia) for the gift of the 1D4 antibody, and Dr. Colin Chu (UCL, Institute of Ophthalmology) for providing an aliquot of the Iba1 antibody.

AUTHOR CONTRIBUTIONS

Conceptualization, RG and MEC Formal analysis, RG and KZ; Funding acquisition, MEC; Investigation, RG and KZ; Methodology, RG, KZ, KH, DP, SEN, AB, RA, MA, DA, DSS, and YL; Project administration, MEC; Resources, MEC; Supervision, MEC; Validation RG and KZ; Visualization; RG and KZ; Writing–original draft; RG, KZ, and MEC; Writing–review and editing, RG, KZ, KH, DP, SEN, AB, RA, MA, DA, DSS, YL, RC, and MEC.

FUNDING

This work was supported by Wellcome Trust (205041/Z/16/Z), Foundation Fighting Blindness (FFB) (FFB-PPA-1719-RAD, FFB PPA-0123-0841-UCL), Fight for Sight, and Moorfields Eye Charity.

COMPETING INTERESTS

The authors declare no competing interests.

ADDITIONAL INFORMATION

Supplementary information The online version contains supplementary material available at https://doi.org/10.1038/s41420-025-02769-2.

Correspondence and requests for materials should be addressed to Rosellina Guarascio.

Reprints and permission information is available at http://www.nature.com/reprints

Publisher's note Springer Nature remains neutral with regard to jurisdictional claims in published maps and institutional affiliations.

(C) (I)

Open Access This article is licensed under a Creative Commons Attribution 4.0 International License, which permits use, sharing,

adaptation, distribution and reproduction in any medium or format, as long as you give appropriate credit to the original author(s) and the source, provide a link to the Creative Commons licence, and indicate if changes were made. The images or other third party material in this article are included in the article's Creative Commons licence, unless indicated otherwise in a credit line to the material. If material is not included in the article's Creative Commons licence and your intended use is not permitted by statutory regulation or exceeds the permitted use, you will need to obtain permission directly from the copyright holder. To view a copy of this licence, visit http://creativecommons.org/licenses/by/4.0/.

© The Author(s) 2025